INTERNATIONAL ATOMIC ENERGY AGENCY
UNITED NATIONS EDUCATIONAL, SCIENTIFIC AND CULTURAL ORGANIZATION

INTERNATIONAL CENTRE FOR THEORETICAL PHYSICS
34100 TRIESTE (ITALY) - P.O.B. 586 - MIRAMARE - STRADA COSTIERA 11 - TELEPHONE: 2240-1
CABLE: CENTRATOM - TELEX 460392 - I

H4.SMR/222 - 20

SECOND AUTUMN WORKSHOP ON
CLOUD PHYSICS AND CLIMATE

(23 November - 18 December 1987)

CLOUD AND PRECIPITATION PROCESSES

Part III

TROPICAL CONVECTION

G.VALI
University of Wyoming
U.S.A.

Workshop in Cloud Physics and Climate

23 November - 18 December 1987

CLOUD AND PRECIPITATION PROCESSES

Gabor Vali
University of Wyoming
U.S.A.

Part III. Tropical Convection.

III. TROPICAL CONVECTION

* Early studies - 1950's Venezuela, Costa rica, ... III/1
* Major field experiments - 1970's AMTEX, BOMEX, GATE, MONEX
* Cloud microphysics - Hawaii, Florida
* Recent projects - Ivory Coast 1982-1985, Hawaii 1985-88, Taiwan 1987

* Most observations over oceans; no topographic effects, global importance.

Boundary layer:

Sea surface (differs from land) - uniform, always wet, slowly changing (large heat capacity, radiation penetrates).

Mixed layer 500-800 m (vs. 1 km over land):
θ_v = const. q = const. III/2

Bouyancy flux decreases with altitude, slightly negative at cloud base III/3

Cloud distributions:

Non-uniform; patches from synoptic to small mesoscale (10-100 km). Due to variations in sea surface temperatures and air mass histories.

Cloud sizes and proportions - larger clouds more slender III/4

Cu fr. - one per 1 km^2; *Cu con.* - one per 1500 km^2 III/5

Case study - GATE Day 261

Off the coast of West Africa. September 18, 1974

Sounding: moist near surface, instability below 800 mb III/6

Cloud distribution from satellite and A/C III/7-8

Radar echo distributions III/9-11

Multiple aircraft penetrations III/12
Moderate, variable updrafts

Model results III/13-15

Cumulonimbus

Major source of precipitation

Updraft and downdraft structures - definitions III/16
diameter, mean and maximum magnitudes at given altitude are log-normally distr. III/17
updrafts are stronger than downdrafts
variations with altitude; updraft peak at mid-level
comparison to continental clouds - tropical weaker III/18

Schematic structure III/19
Wide, well-defined updraft at leading edge
Updrafts narrower, stronger aloft
Coincident with precipitation aloft there are mixed up and downdrafts
In precipitation at the ground there is wide downdraft; produces gust outflow.

Mesoscale systems

Convective cloud clusters III/20
Slow motion - few meters per second
Evolution from major cells to stratiform precipitation over 2-6 hours

Squall systems III/21
Fast moving - 15 m s^{-1}
Sharp leading edge, line or arc
Strong cells followed by stratiform precipitation within ~ 100 km. Mesoscale lifting above 0°C level.
Steady state.

Hurricanes

Precipitation and cloud processes

Precipitation at the ground - rain III/22-23

Ice particles observed aloft
Convective clusters III/24
Squall line III/25-26
Hurricane III/27-29

Considerable similarity to extratropical storms
Ice multiplication contributes
Riming in convective regions
Vapor growth and aggregation in stratiform region
Melting band in stratiform region

III/1

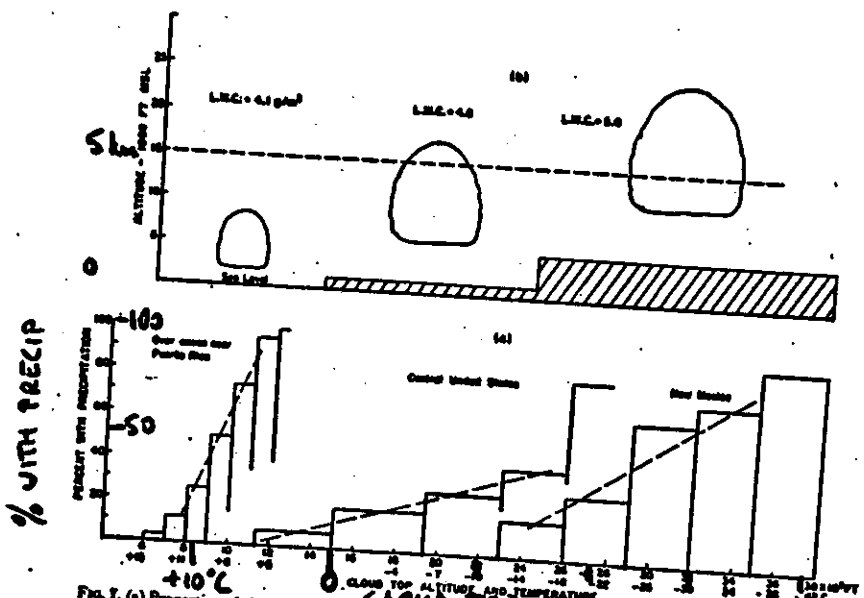

FIG. 7. (a) Proportion of visually observed clouds that yielded a radar echo and so were assumed to be precipitating, plotted against height above sea level and a temperature scale adjusted to be representative in all regions. (b) Size and calculated maximum liquid water content of that class of cloud of which 20 percent yielded radar echoes (from Battan, Byers, and Braham, 1955).

Table 1. Cloud depths related to the frequency occurrence of radar echoes.

Caribbean Sea (warm clouds) (after Byers and Hall)		New Mexico (after Braham et al)	
Cloud depth (ft)	Per cent of clouds with echoes	Cloud depth (ft)	Per cent of clouds with echoes
3,500—4,000	2		
4,000—4,500	4		
4,500—5,000	11		
5,000—5,500	13		
5,500—6,000	23		
6,000—6,500	28	> 5,000—8,000	0
6,500—7,000	33		
7,000—7,500	47		
7,500—8,000	73		
8,000—8,500	74		
8,500—9,000	83	> 8,000—11,000	16
9 000 and up	100	> 11,000—14,000	30

Tolbo X (1938), II

III/2

M. A. LeMone, 1980

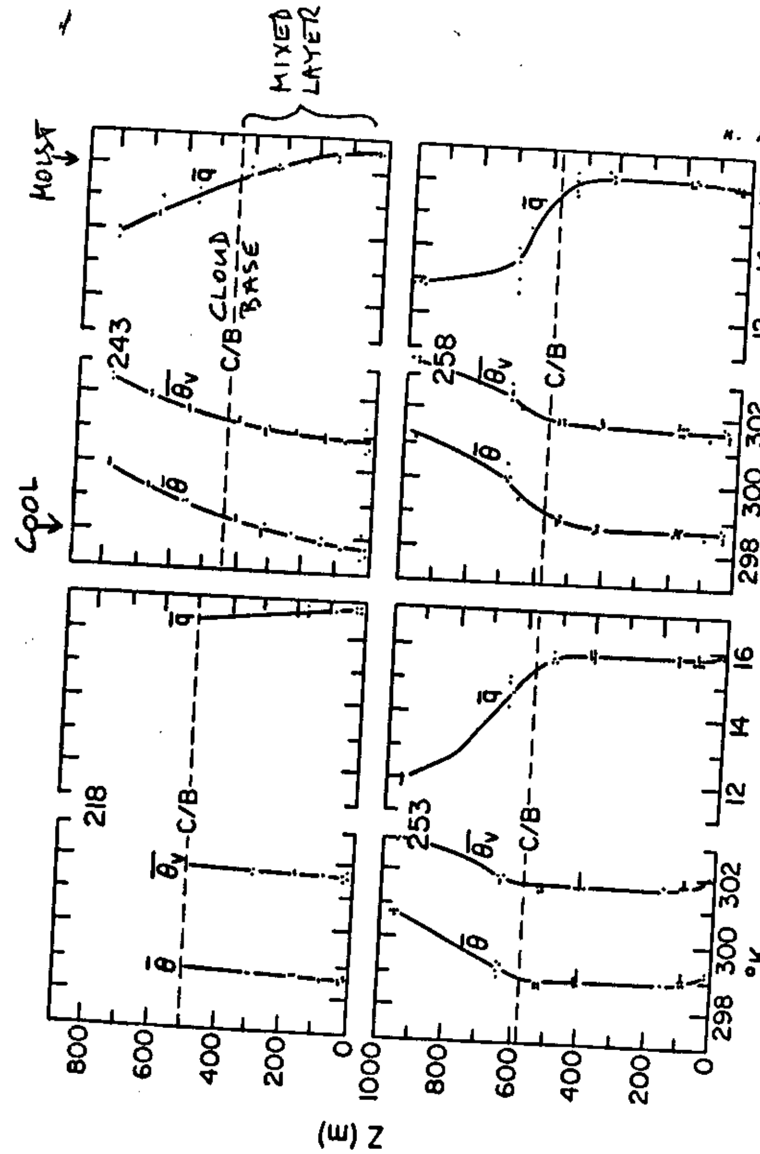

Fig. 1 Profile of potential temperature, θ; virtual potential temperature, θ_v; and specific humidity, q, for 4 days in GATE (Day 218 = 6 Aug.; Day 243 = 31 Aug.; Day 253 = 10 Sept.; Day 248 = 15 Sept., all 1974).

III/3

Lemone, 1980

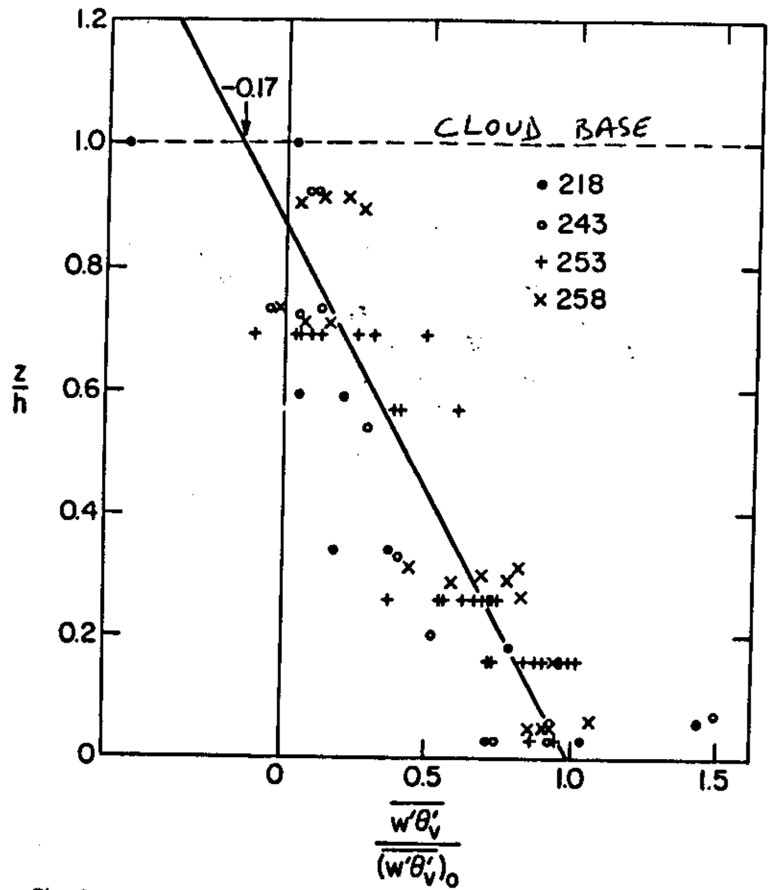

Fig. 3 Profile of virtual potential temperature flux $\overline{w'\theta_v'}$, normalized by corresponding surface values, $(\overline{w'\theta_v'})_0$, for the 4 GATE days of Fig. 1. The straight line through the data represents an objective least squares fit, constrained to go through 1.0 at the surface.

III/4

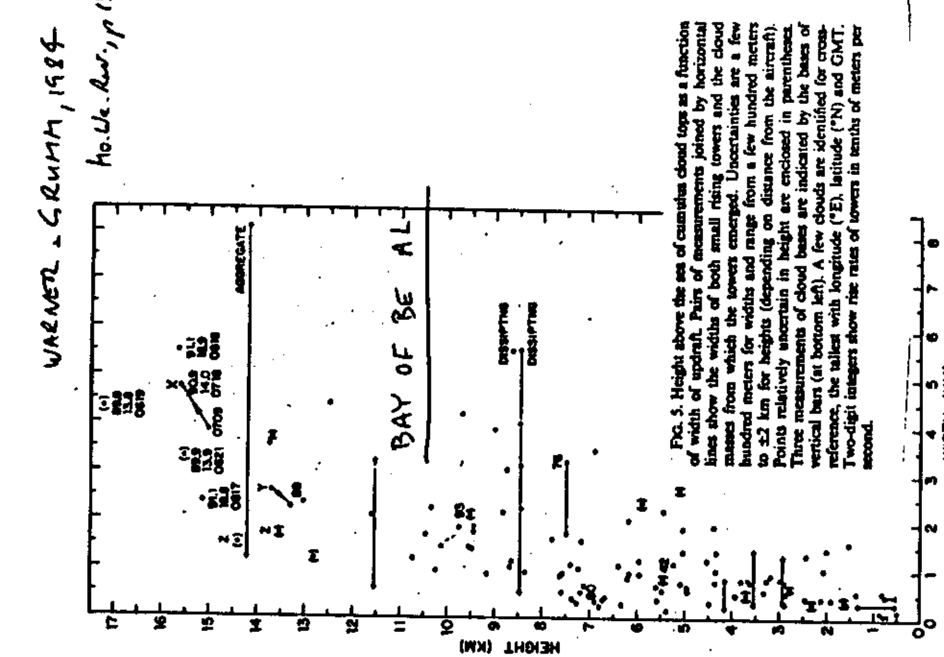

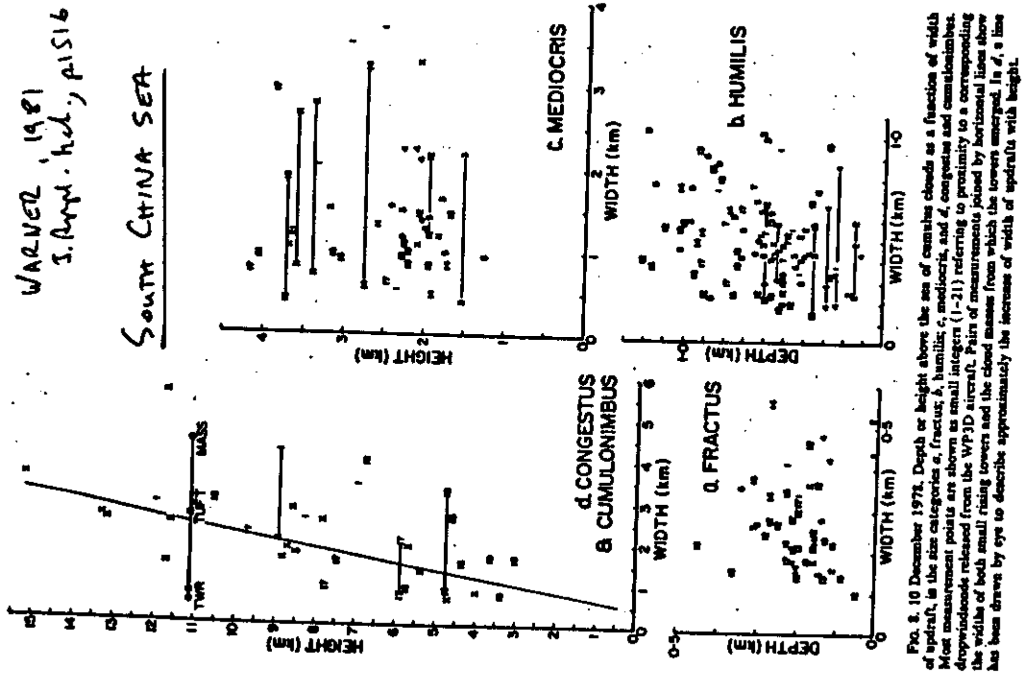

WARNER & GRUMM, 1984
Mo. Wea. Rev., p153

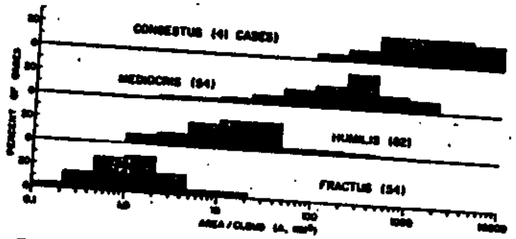

CLOUD DENSITIES
*

FIG. 7. Histograms of inverse cloud number densities, or horizontal areas per cloud, in the categories fractus, humilis, mediocris and congestus. The uncertainty is nominally a factor of 2.

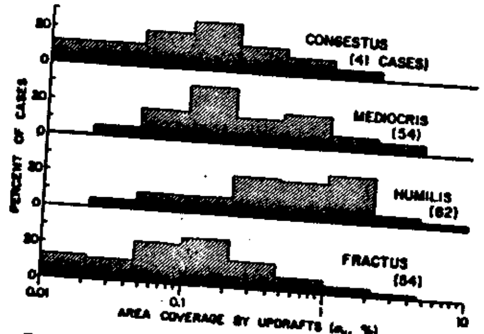

UPDRAFT AREAS
**

FIG. 8. Histograms of percent area coverage by updrafts σ_u. Categories as in Fig. 7. The uncertainty is nominally a factor of 10.

TABLE 3. Median values of inverse cloud number densities, area coverages by updrafts and area mean ascent rates for different size categories of cumulus.

Cumulus category	Fractus	Humilis	Mediocris	Congestus
Approximate height of assessments (km)	0.7	1	2	4
Median area of assessments (km^2)	18	120	770	3000
* → Median A (km^2 cloud^{-1}) (Fig. 7)	1.1	14	220	1500
Median width of cloud updraft (m)	40	300	800	1500
** → Median σ_u (%) (Fig. 8)	0.10	0.54	0.20	0.11
Stipulated mean updraft speed (m s^{-1})	small	1.0	2.5	2.5
Median ω (Pa s^{-1}) (Fig. 9)	small	−0.06	−0.05	−0.02 ← AREA MEAN ASCENT

GATE DAY 261

OLLI TURPEINEN AND MAN KONG YAU 1981
Mo Wea Rev p1495

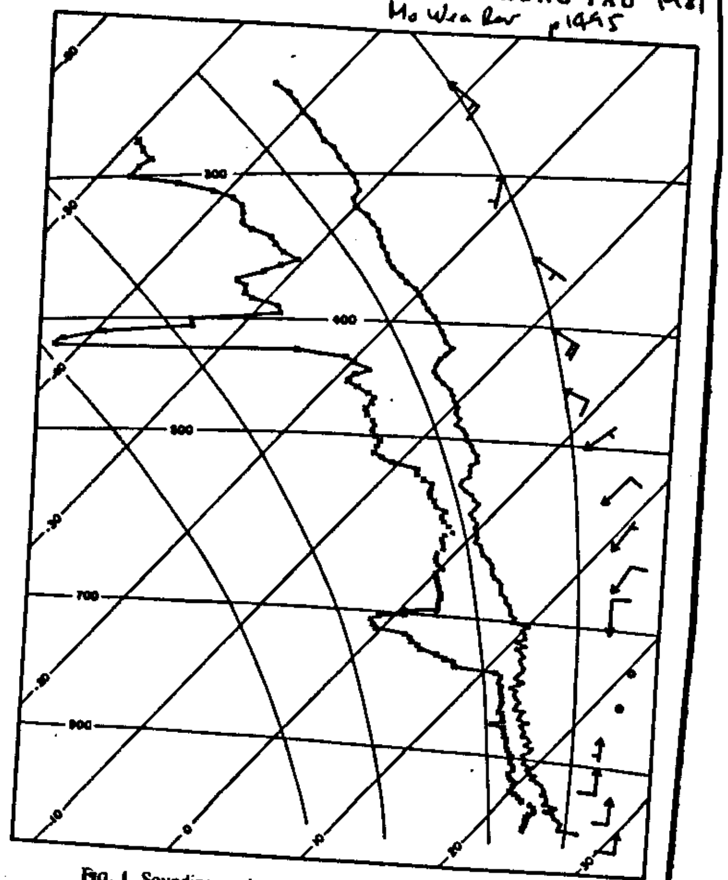

FIG. 1. Sounding made at 1200 GMT plotted on a tephigram.

II/17

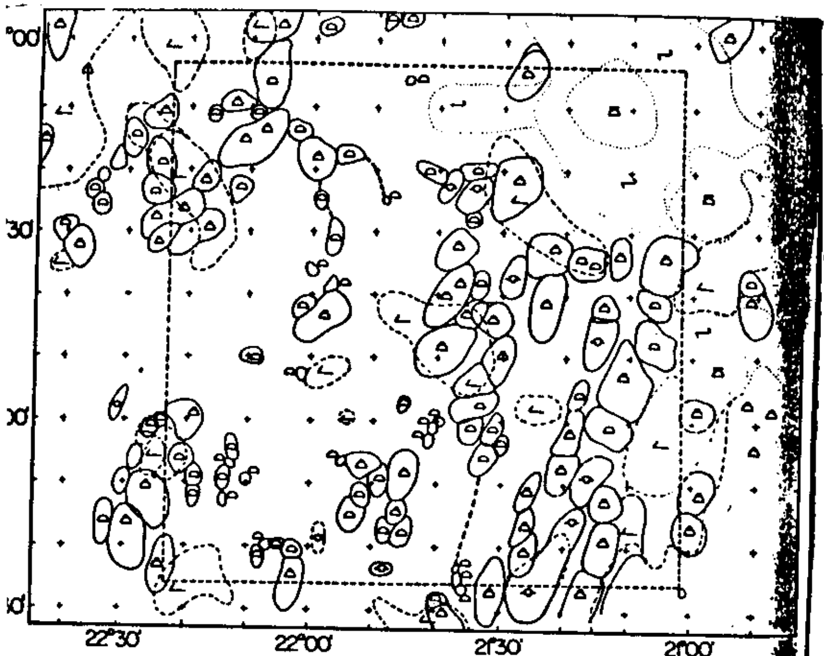

...o. 1. 1352 GMT. Cloud coverage from a map of digital cloud brightness in the visible channel of SMS-1. All clouds resolved ...s contoured digital data, of resolution ~2 km, are represented. Solid lines show cumulus (including stratocumulus), dashed ... show stratiform and dotted lines show cirriform clouds. Heavy dashed lines mark lines of very small cumulus. Divisi... ...een adjacent clouds are based on brightness gradients. Cloud type was determined by viewing sequences of full resol... ...le and infrared images centered on 1352 GMT. The box marks the track of the aircraft.

GATE 261

Warner et al. 1980 M. Weather Rev. p 169

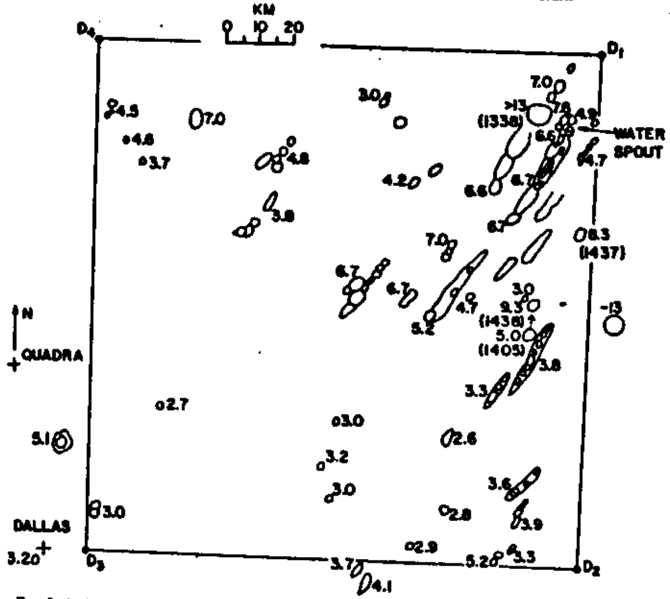

FIG. 2. Active cloud tops (outlined by contours) in the height interval 2.5 to >13 km, during the first ...ox circuit by the aircraft, 1300–1445 GMT. Numbers are heights (km) above the sea, and times of ...easurement. The corners D_1 to D_4 define the box circuit, between latitudes 8°34' and 9°56'N, and ...ongitudes 21°2' and 22°23'W. A detail of the original of this figure appears in Fig. 3.

II/18

GATE 261

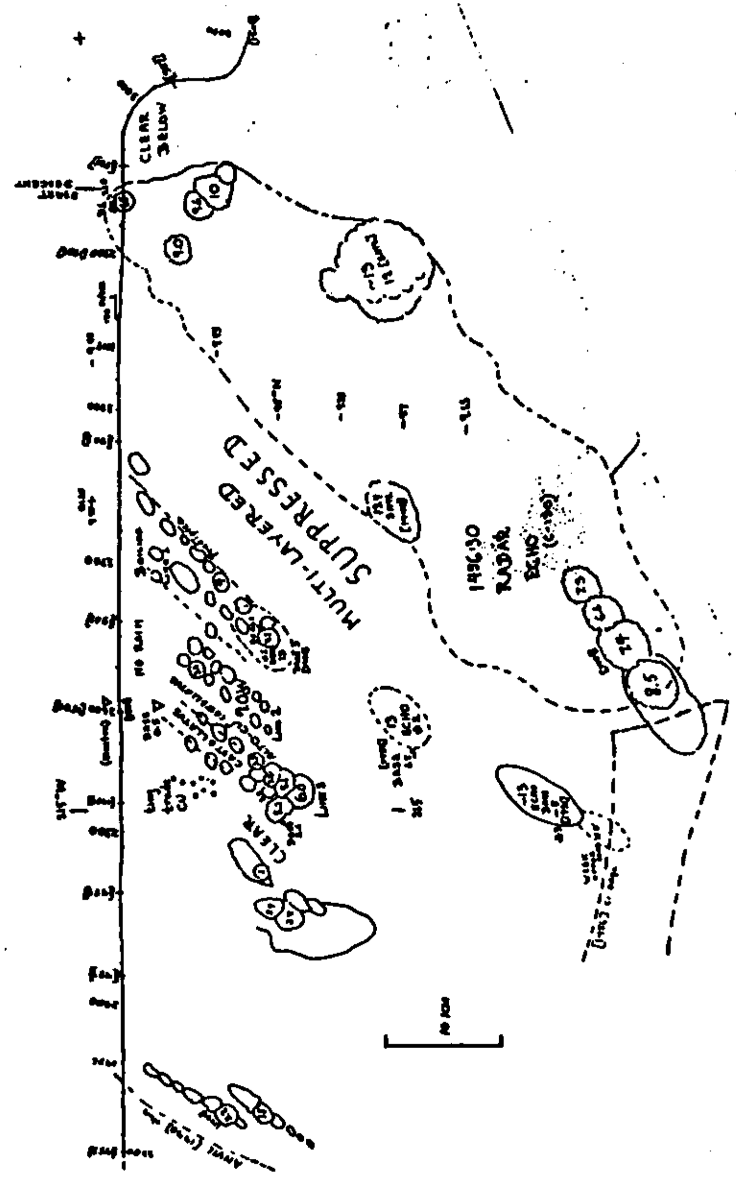

FIG. 3. 1444 to 1508 GMT. Clouds near D_1 (at the northeast corner of the box), mapped by photogrammetry from the US-C130. Rounded clouds are active cumulus drawn to scale. C130 radar and satellite data are included.

TURPEINEN & YAO, 1981 Mo Wea Rev p. 1495

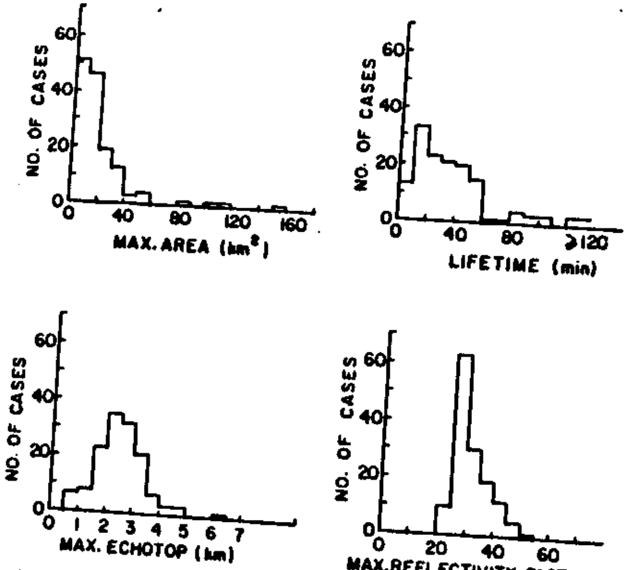

FIG. 2. Frequency distributions of maximum area, lifetime, maximum echo top and maximum reflectivity factor for the whole echo population.

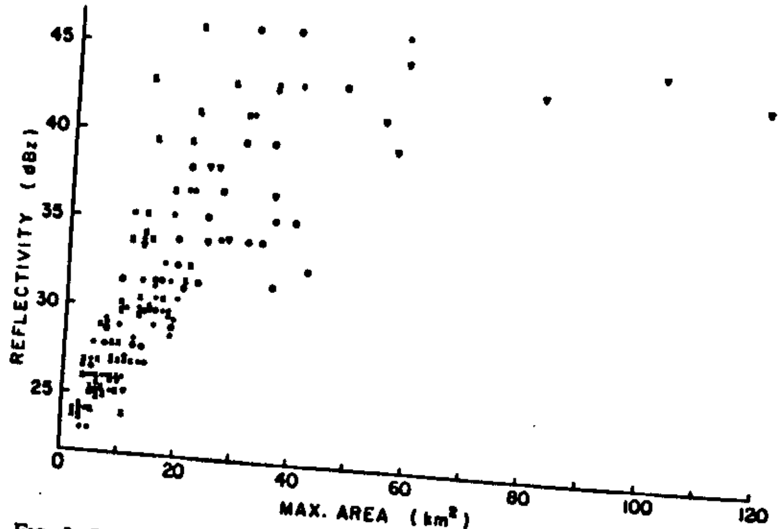

FIG. 3. Scatter diagram of the correlation between maximum area and maximum reflectivity factor: (×) isolated cells, (●) relatively isolated cells, (O) cells close to another cell, (▼) merging cells. Note that the y axis starts from 22 dBZ.

C. WARNER AND G. L. AUSTIN, 1978 Mo. Wea. Rev. p. 983

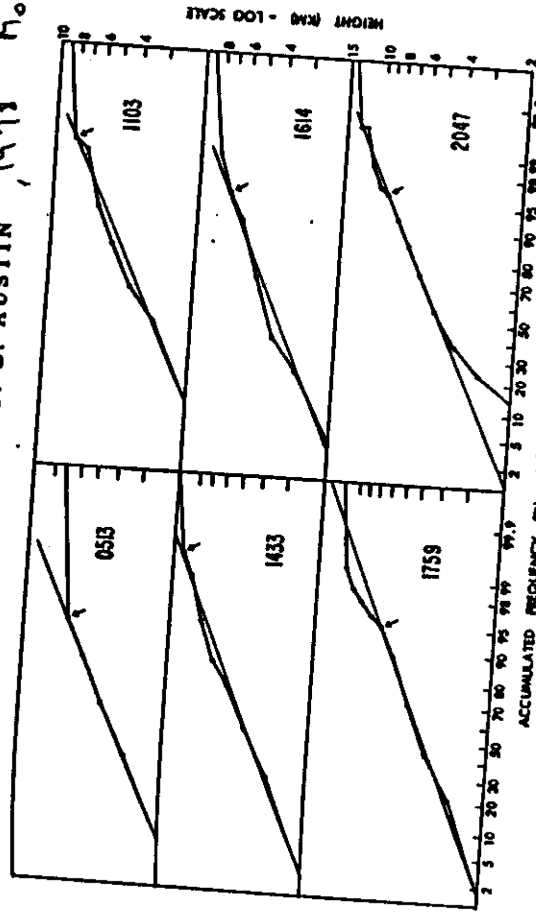

FIG. 7. Echo top heights. Cumulative probability distributions of peak echo top heights in radar bins of area 17.6 km² for different times as indicated. Straight lines of log-normal distributions are drawn in by hand. Arrows indicate approximate upper limit of log-normality.

TURPEINEN & YAO 1981

GATE 261
3D MODEL
CELL GROUPS

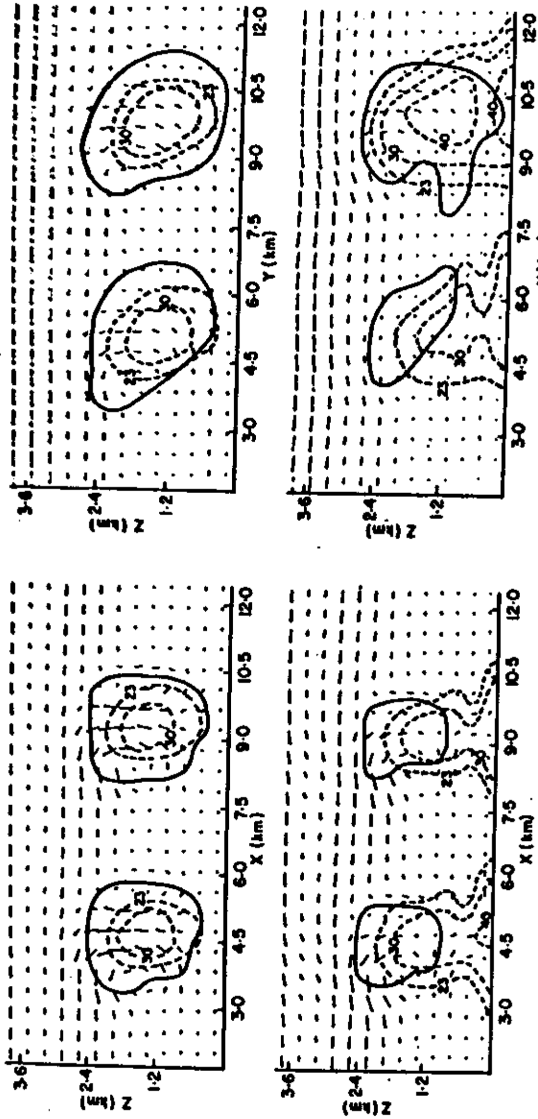

FIG. 10. Vertical cross sections through the centers of the initial impulses of vector velocity, cloud water content and radar reflectivity factor for the perpendicular cells in run VII (left) and the parallel cells in run VIII (right) at 20 (top) and 30 min (bottom). The spacing of the contours and the normalization of the arrows are the same as in Fig. 9.

GATE 261 2D MODEL

FIGURE 2

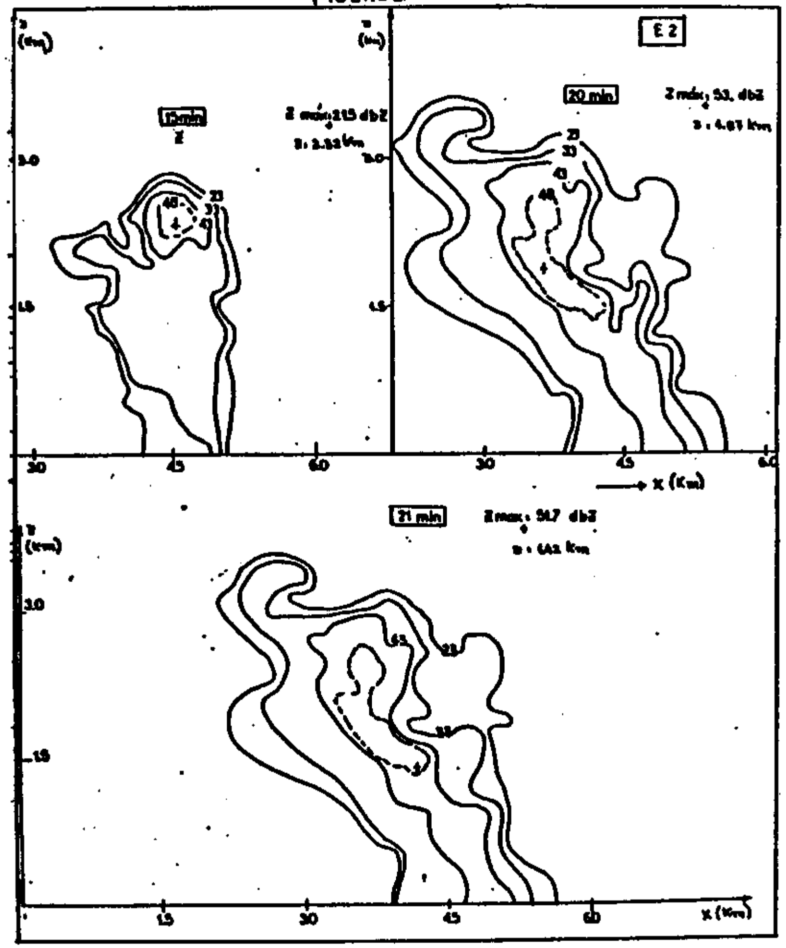

III/11

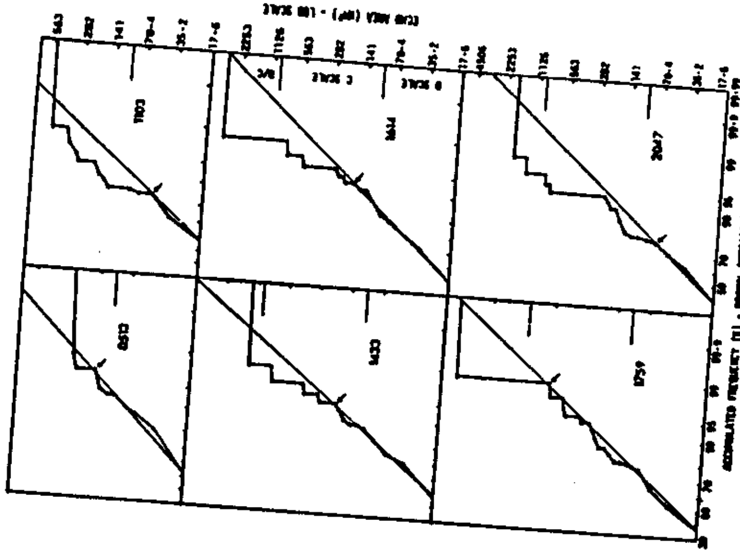

Fig. 8. Echo areas. Cumulative probability distributions for times as indicated. Straight lines of log-normal distributions are drawn in by hand. Arrows indicate approximate upper limit of log-normality.

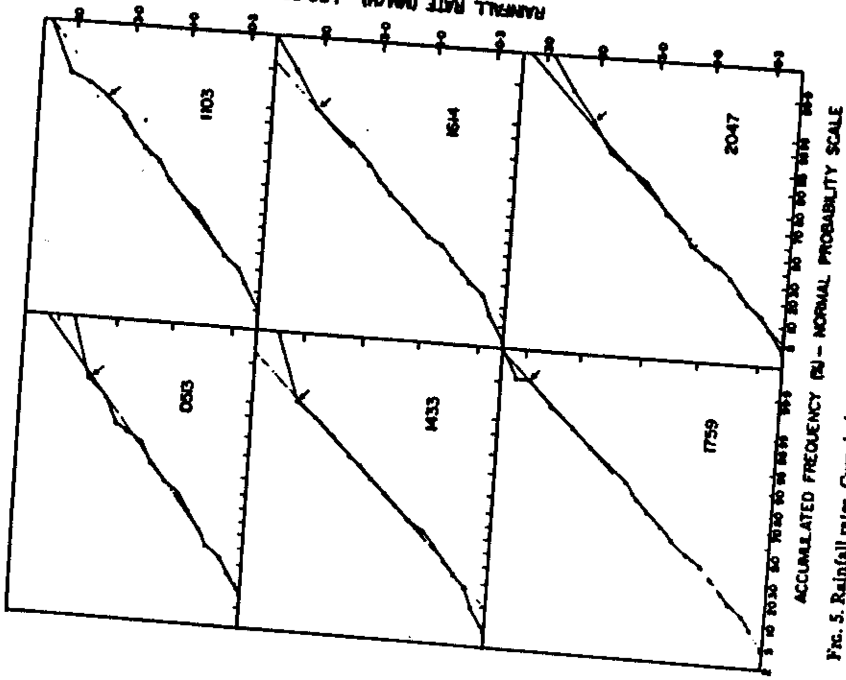

Fig. 5. Rainfall rates. Cumulative probability distributions of rainfall of different rates in radar bins of area 17.6 km² for different times as indicated. Straight lines of log-normal distributions are drawn by hand. Arrows indicate approximate upper limit of log-normality.

II/12

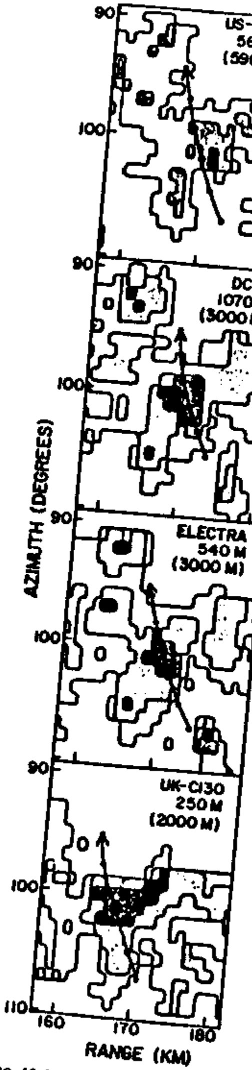

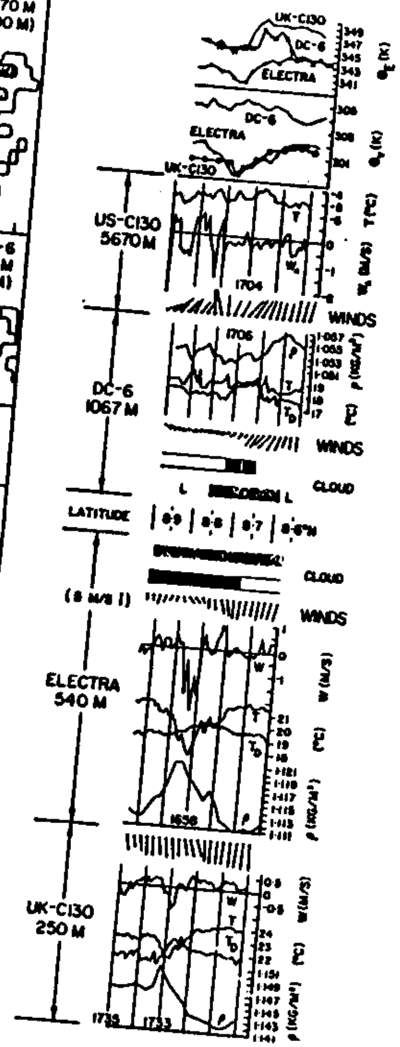

Fig. 15 (Left). Tracks of four aircraft through radar echo group P. Dots are at minute intervals, comparable with Fig. 16. Flight altitude is shown, and approximate altitude of radar scan is in parentheses. Maps are elements of B-scans with coordinates of azimuth and range from the *Quadra* radar. For the location of group P see Fig. 11 (bottom right). Reflectivity contours at 23, 27, 34 and 44 dBZ. Profiles of reflectivity shown in Fig. 13e.

Fig. 16. (Right). Time-series plots of data from four aircraft, penetrating echo group P (Fig. 15). The plots are keyed to geographical location, shown in the middle. See text for details. Winds are represented by barbs: a wind of 5 m s^{-1} from 180° is as shown in parentheses at middle left. Under CLOUD, the letters C and L mean flight environments of cumulus clouds and clear air, respectively. Dense shading indicates flight within dense cloud; bars without shading indicate flight within tenuous cloud. Such observations are not given for the C130's.

III/15

WMO WORKSHOP
IRSEE 1985

MODEL - OBSERVATION INTERCOMPARISON

Case: Gate 261

Undisturbed conditions with small-moderate cumulus.
Deeper clouds later in day.

PARAMETER	OBSERVATION	Turpeinen 3d) MODEL	(Nicolini 2d)	(Ou 1d)
CLOUD TOP	3 km	3.3 km	3 km	2.1 - 7km
CLOUD LIFETIME	20-60 min	35 min	30 min	28-60 min (to reach top)
CLOUD DIMENSION	4 km (typic.) 10 km (some)	5 km	1.5 km	
UPDRAFT MAGNITUDE	2 ms^{-1} (cloud base)	5.7 km at 2.1km	5.9 km at 2.0 km	
DOWNDRAFT MAGNITUDE		3.4 km at 3.0 km	4.6 km at 2.4 km	
CLOUD WATER	1.6 g/m^{-3} (max) at 1.1 km	2.4 g/m^{-3} (max) at 2.25 km	3.2 g/m^{-3} (max) at 2.5 km	
PRECIP AT GROUND	2 mm hr^{-1} (typ) 20 mm hr^{-1} (max)	36 mm hr^{-1} (max)	9 mm hr^{-1} (max)	2-23 mm hr^{-1}
RADAR ECHO	45 dbz (max)	48 dbz (max)	42 dbz (max)	
CLOUD MOVEMENT	variable	N wards with 900 mb wind	N wards very slow	

1d SIMULATION SENSITIVE TO MIXING AND INITIAL RADIUS

III/16

LEMONE & ZIPSER, 1980
J. Atm. Sci., p.2444

GATE, 1974

WEST COAST AFRICA

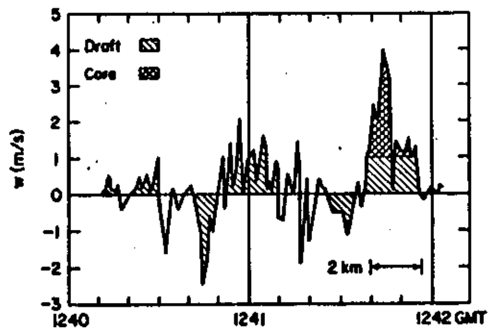

FIG. 2. Time series illustrating definition of drafts and cores, adapted from US C-130 at 5471 m, Day 257. An updraft has to reach 0.5 m s^{-1} and be positive for 0.5 km (~5 s) or more; a core has to have w of at least 1 m s^{-1} for 0.5 km or more. Downdrafts and downdraft cores are defined in the same way. Note that the draft at the right has two cores.

⇐ EXAMPLE

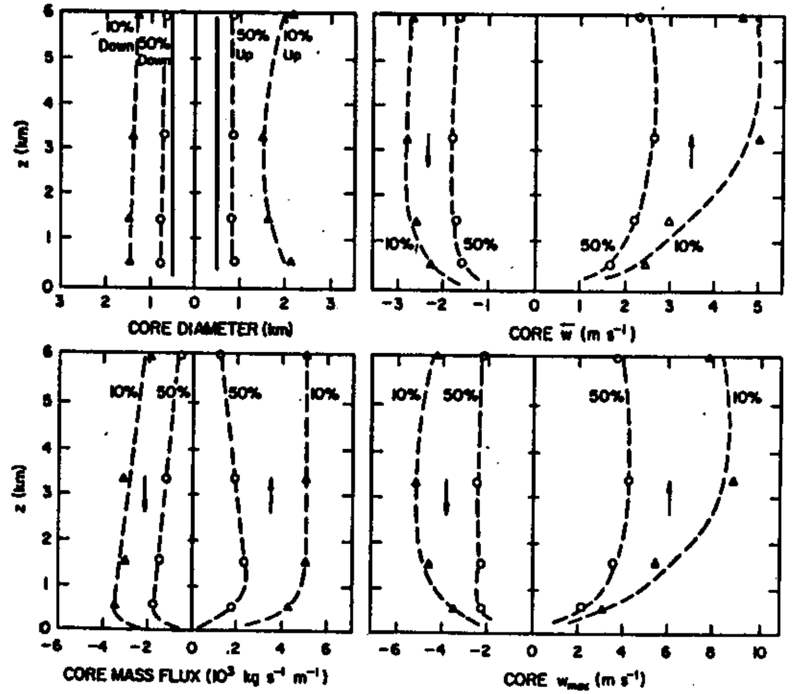

FIG. 5. Variation with altitude of median (50%) and 10% level (stronger than 90% of the population) updraft and downdraft cores, with respect to core diameter, mean vertical velocity of cores, maximum 1 s vertical velocity within core, and core mass flux.

⇐ STATISTICS

GATE, 1974

DETAILED STATISTICS FOR ONE ALTITUDE RANGE

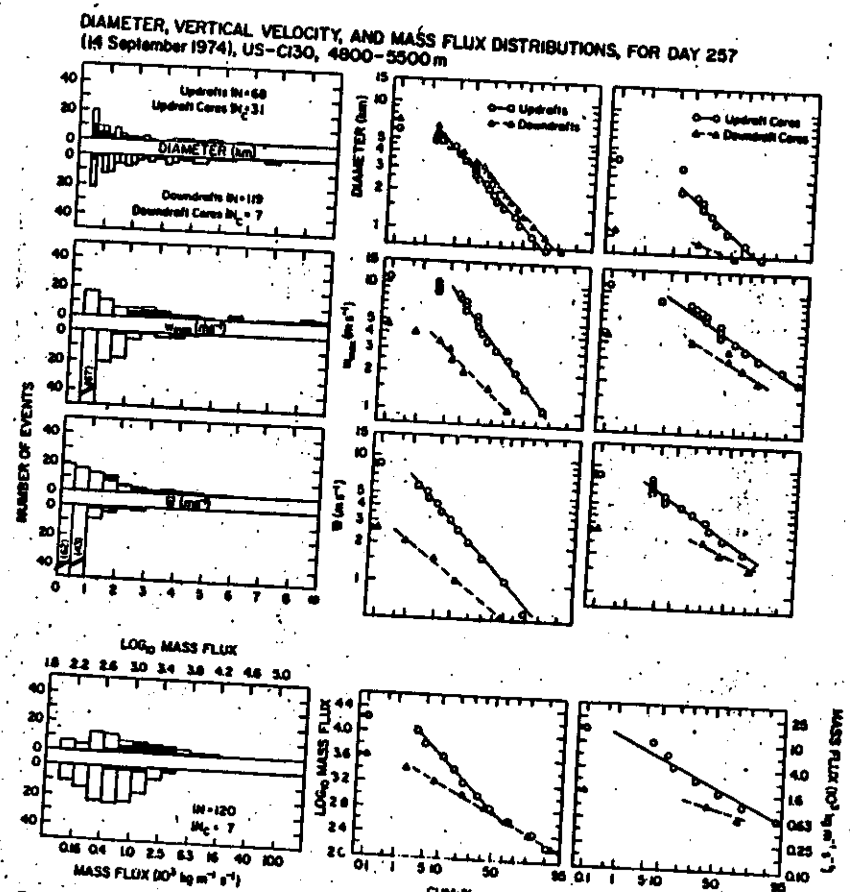

FIG. 3. Diameter, vertical velocity and mass flux distributions for Day 257 (14 September 1974), at 4800–5500 m, from the US C-130. In the left column of the figure, the upward extending bars of the graph are for updrafts, the downward extending bars are for downdrafts. For updraft: (1) ▭ bars: total length is total number of drafts; black is number of cores; (2) ▬ bars: total length is total number of cores; clear, number of drafts. Downdrafts and downdraft cores are coded analogously. Cumulative distributions for drafts are in the middle column; cumulative distributions for cores are in the right column.

COMPARISON OF GATE DATA WITH CONTINENTAL DATA, EASTERN U.S.

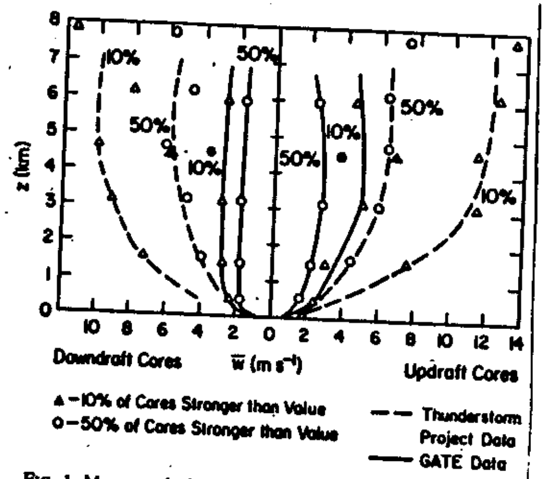

FIG. 1. Mean vertical velocity in updraft and downdraft cores as a function of height, comparing different data sets. The GATE data for strong (10% level) and median (50% level) cores are taken from Fig. 5 of LZ. The Thunderstorm Project Data defined in the same way are adopted from Byers and Braham (1949), Tables 7 and 10. For the 4.5 km level only, data from Gray (1965), Fig. 13, defined similarly, are included (filled symbols).

IV

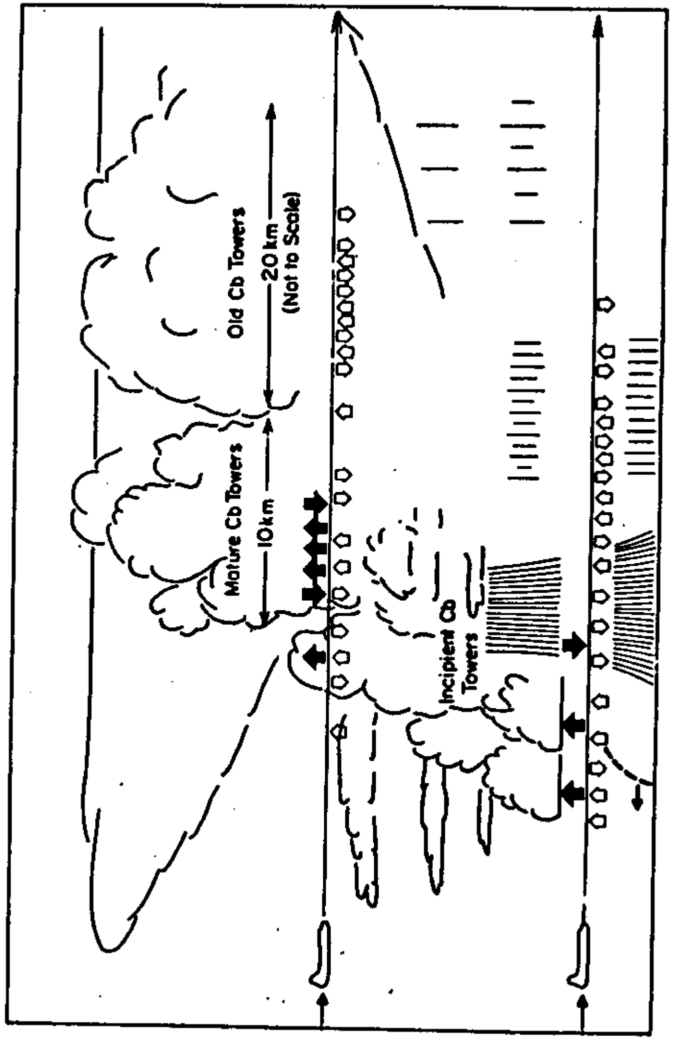

FIG. 4. Schematic of "typical" aircraft passes through a convective band, showing location of drafts and cores near cloud base and in the middle troposphere. There are wide variations from day to day and from one pass to the next on any given day. An average leg is 90 km in length, half of which would be involved with clouds and precipitation and which would contain most of the drafts and cores.

Altogether the four stages last about a day, the convective circulations dominating in the early stages and the mesoscale circulations dominating in the later stages.

III/20

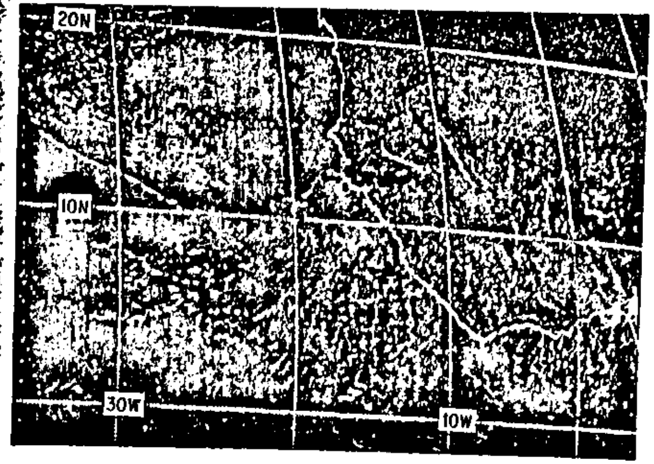

Figure 14. Visible photograph from the SMS-1 geostationary satellite at 1130 GMT on 5 September 1974, showing tropical cloud systems ranging from fields of small cumulus to large cloud clusters. Cloud clusters are evident from their large cirrus shields at 9°N 24°W, 9°N 21°W, 7°N 16°W, 8°N 12°W, and 14°N 13°W. The last of these was a squall cluster with an arc cloud line on its leading (southwest) side (From Houze & Hobbs[33])

CLOUD CLUSTERS

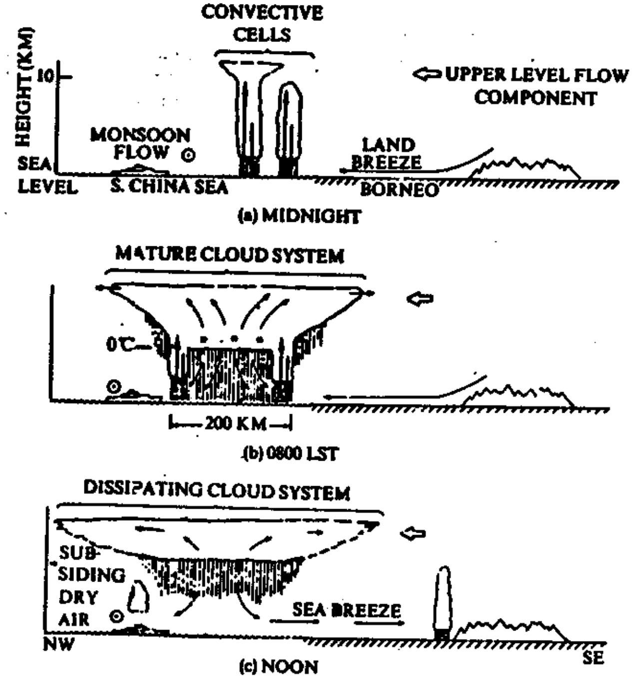

Figure 15. Schematic depiction of the development of a diurnally generated non-squall tropical cloud cluster off the coast of Borneo. Various arrows indicate airflow. The circumscribed dot indicates northeasterly monsoon flow out of the page. The wide open arrow indicates the component of the typical east-southeasterly upper-level flow in the plane of the cross-section. Heavy vertical arrows in (a) and (b) indicate cumulus-scale updraughts and downdraughts. Thin arrows in (b) and (c) show a mesoscale updraught developing in a mid- to upper-level stratiform cloud with a mesoscale downdraught in the rain below the middle-level base of the stratiform cloud. Asterisks and small circles indicate ice above the 0°C level melting to form raindrops below this level (From Houze et al.[34])

II/21

SQUALL SYSTEM

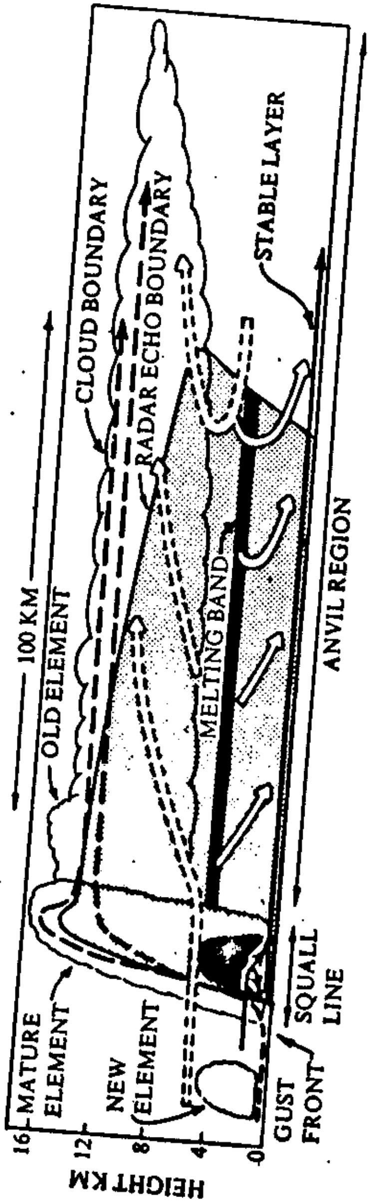

Figure 13. Schematic depiction of a typical cross-section through a tropical squall system. Dashed and continuous streamlines, respectively, show convective-scale updraughts and downdraughts associated with the mature squall-line elements, and also their inflows and outflows. Wide dashed and solid arrows, respectively, show mesoscale updraught and downdraught circulations. Dark shading shows strong radar echo in the melting layer and the heavy precipitation zone of the mature squall-line element. Light shading shows the weaker radar echoes. The scalloped line indicates the visible cloud boundary (From Houze & Hobbs [32])

II/22

COMPARISON OF PRECIP. AT GROUND

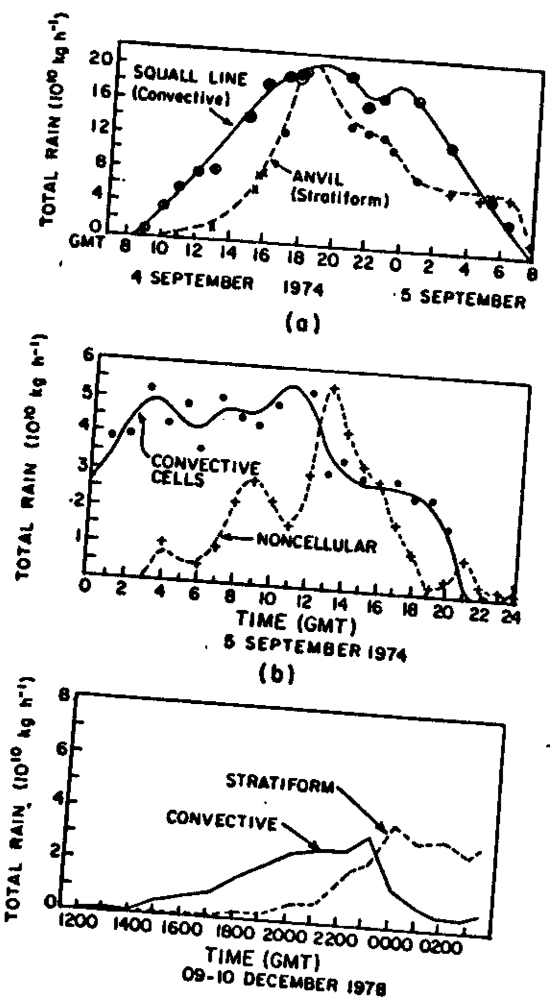

SQUALL

CONVECTIVE CLUSTERS

FIG. 41. Time variation of total rain integrated over areas covered by the convective and nonconvective regions of (a) a squall cluster and (b) and (c) two nonsquall clusters. The squall-line case is from Houze (1977). The nonsquall cases are from Leary (1981) and Churchill (1982).

AUSTIN & GEOTIS, 1976
J. Appl. Meteor., p 569

RAIN AT SURFACE

GATE

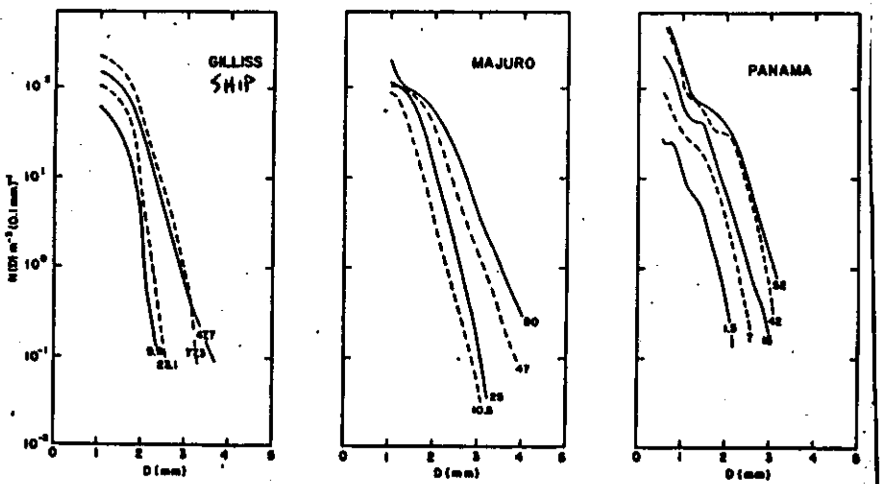

FIG. 3. Examples of averaged drop size distributions from various locations. [Majuro data from Mueller and Sims (1967); Panama data from Gentis (1968).]

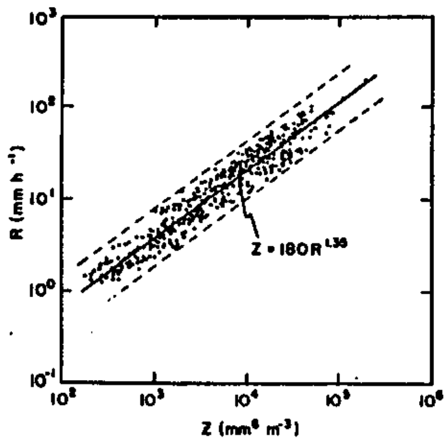

FIG. 5. Relation between rainfall rate and radar reflectivity factor for all data points. Lines show best fit by eye and region within a factor of 2 in rainfall.

HOUZE & CHURCHILL, 1984, JAS p3405

WINTER MONSOON CLOUD CLUSTER

SOUTH CHINA SEA, 9 CASES, DEC, 1978

7-8 km; −14 to −19°C

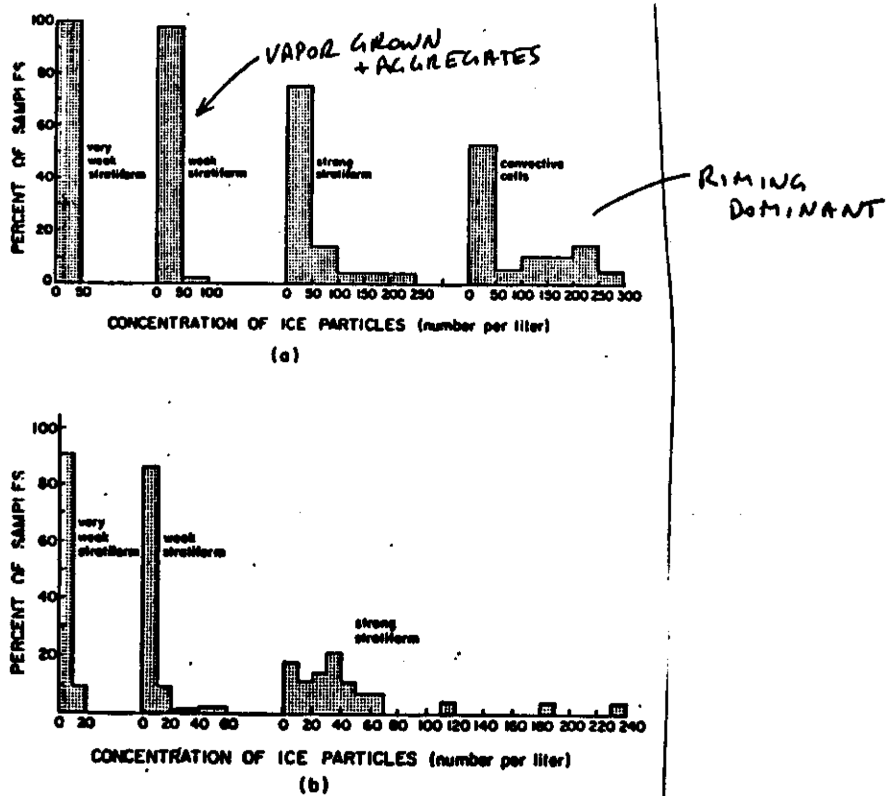

FIG. 1. Concentrations of particles observed with the PMS cloud probe (upper particle size limit 1.6 mm) aboard the NOAA WP-3D aircraft during Winter MONEX. Observations were made at altitudes of 7–8 km (−14 to −19°C) and the concentrations referred to were 1 min averages. The categories very weak stratiform, weak stratiform, strong stratiform and convective cells describe the precipitation through which the aircraft was flying. In (a) an increment of 50 per liter on the abscissa was used in plotting the histograms. In (b) an increment of 10 per liter was used to show more detail in the stratiform categories.

BAY OF BENGAL DEPRESSION

Houze & Churchill, 1987, J. Atm. Sci.

5 JULY
1979

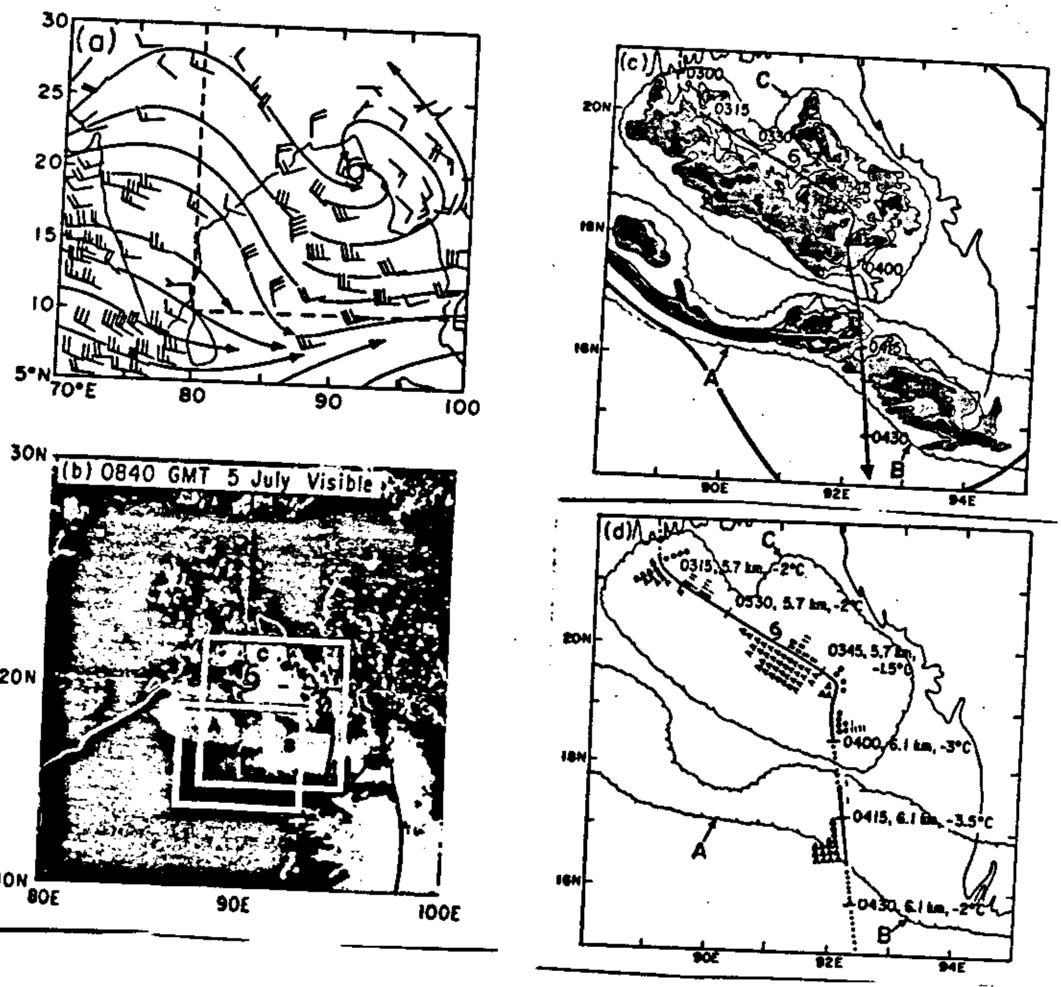

III/25

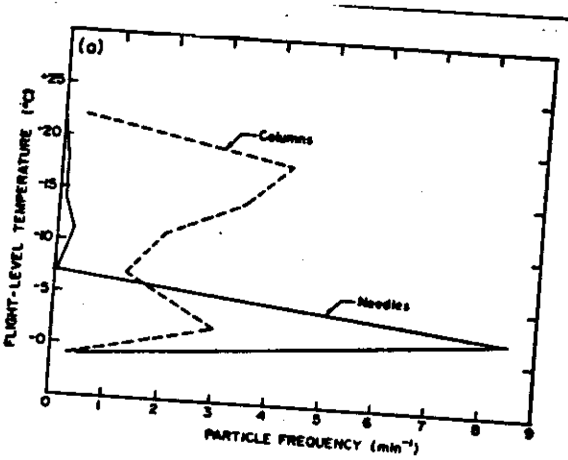

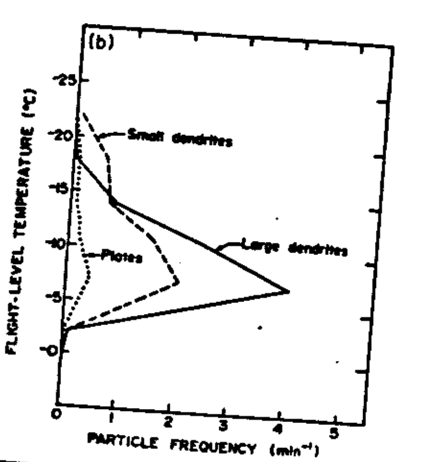

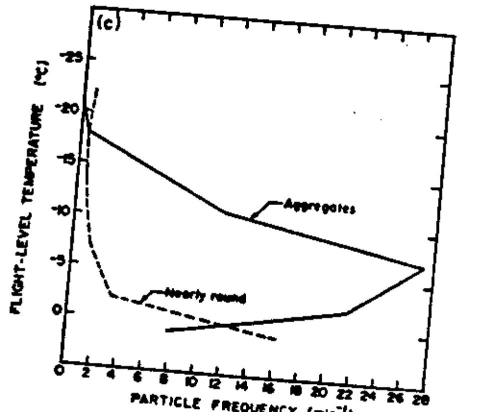

FIG. 7. Vertical distribution of hydrometeor frequencies. The number of hydrometeors of a habit observed for each minute of in-cloud flight time are plotted against the flight-level temperatures at which they were observed. Data represent the entire case study of 3, 5, 6, 7 and 8 July. (a) Columns and needles. (b) Small dendrites, large dendrites, and plates. (c) Aggregates and nearly round particles.

III/26

BLACK & HALLETT, 1986
J. Atm. Sci p. 802

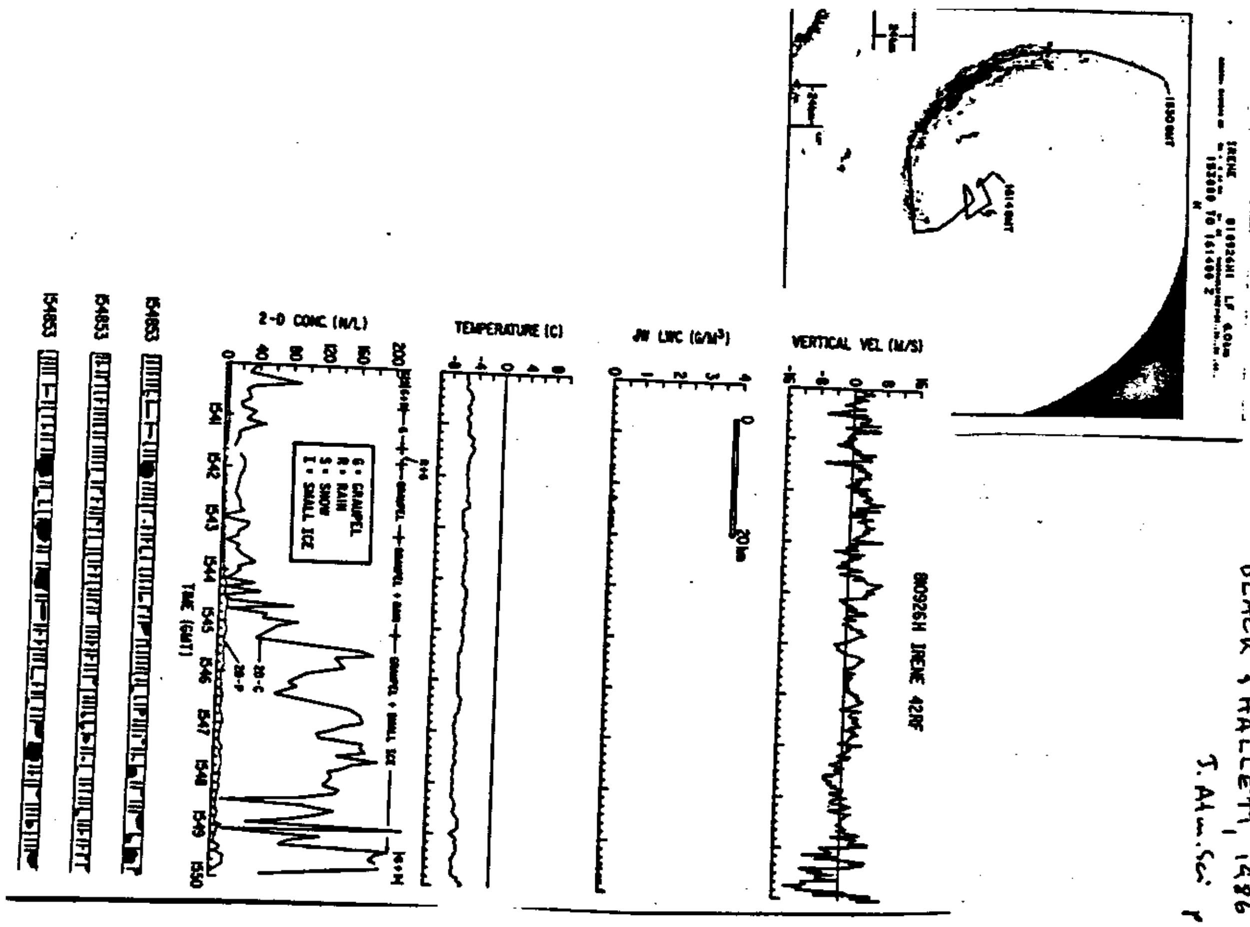

Black & Hallett

TABLE 2. A synopsis of the vertical velocity, JW liquid water content, and 2-D particle concentration data gathered in three Atlantic hurricanes.

Category	Number up	$\overline{V_w}$ (m s^{-1})	$\overline{JW_{max}}$ (g m^{-3})	No. 2-D samples	Mean concentration (L^{-1}) 2D-P	2D-C	$\overline{V_w}$ (m s^{-1}) (with rain)	Number of samples with rain
				*Updrafts**				
$T \le -5°C$, $JW > 0$ g m^{-3}	150	4.0	0.3	57	5.8	37.8	8.4	22
$T \le -5°C$, $JW \ge 0.5$ g m^{-3}	33	7.1	0.9	6	3.3	23.5	11.2	5
$-5°C < T \le -2°C$, $JW > 0$	116	4.1	0.5	46	4.1	15.9	7.3	16
$-5°C < T \le -2°C$, $JW \ge 0.5$ g m^{-3}	34	7.4	0.9	16	4.1	16.8	9.8	7
$T > -2°C$, $JW > 0$ g m^{-3}	84	3.5	0.3	41	4.7	13.2	6.4	33
$T > -2°C$, $JW \ge 0.5$ g m^{-3}	41	12.9	0.8	25	3.7	19.7	14.6	25
$T \le -5°C$, $JW = 0$	118	3.0	0	25	2.0	37.3	7.5	3
$-5 < T \le -2°C$, $JW = 0$	105	2.2	0	30	1.9	11.8	6.6	2
$T > -2.0°C$, $JW = 0$	76	2.3	0	7	1.8	3.3	2.6	7
				*Downdrafts***				
$T \le -5°C$	24	−3.6	<0.1	13	8.9	76.7	—	—
$-5 < T \le -2°C$	39	−3.3	<0.1	30	6.5	36.2	—	—
$T > -2°C$	83	−2.7	<0.1	17	3.2	15.1	—	—

* In columns 3 and 8 $\overline{V_w}$ and $\overline{V_w}$ are maximum in updrafts.
** In columns 3 and 8 $\overline{V_w}$ and $\overline{V_w}$ are minimum in downdrafts.

Black & Hallett III/29

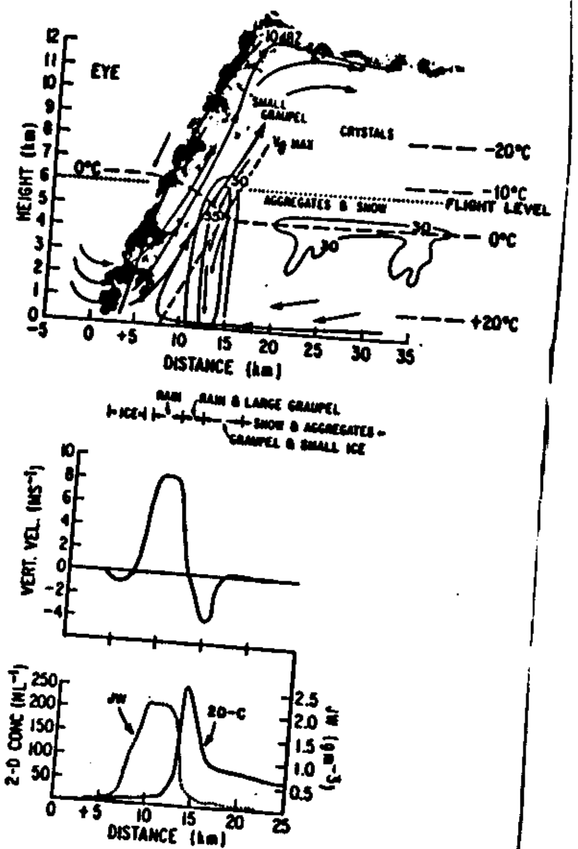

FIG. 14. Schematic of the strong eyewall updraft-downdraft in radial cross section, showing the location of the updraft with respect to the eyewall and principle rainband. The concentration and particle phase indications represent what would be typically found in a penetration across such a feature at a level at or <2 km above the altitude of the melting level in the outer regions of the storm. Ice particles on the inner edge of the convection were only found in the radial penetration of the Irene rainband. That penetration was the only one made where the inner edge was colder than 0°C.